JMEPEG (2005) 14:293-300
DOI: 10.1361/10599490523878

1059-9495/$19.00

Machining Cancellous Bone Prior to Prosthetic Implantation

M.J. Jackson, G.M. Robinson, H. Sein, W. Ahmed, and R. Woodwards

(Submitted January 3, 2004; in revised form February 25, 2005)

The structure of cancellous bone can be described as heterogeneous, and as such, is difficult to shape by cutting tools during clinical surgical practices. The structure of bone can have a devastating effect on the performance of the cutting tool unless it is coated with a hard-wearing, thin solid film. Here, the use of diamond-coated cutting tools to prepare bone for biomedical implants are investigated. This paper describes developments in the use of coated cutting tools for machining of cancellous bone and to prepare a nanostructured surface.

Keywords biomedical applications, cancellous bone, coated cutting tools, diamond

1. Introduction

The structure of cancellous bone (i.e., bone with a relative density less than 0.7) is made up of an elaborate sandwich of compact dense bone on the outer shell and a core of porous, cellular material. This configuration minimizes the weight of the bone over a fairly large load-bearing area. As patients become older, weight loss can result in fractures that can be alleviated by using implants at an earlier age. However, the cancellous bone that is replaced is thought to be a primary cause of osteoarthritis in older patients and so implants must match the bone it replaces. When replacing cancellous bone, the area to be removed must be replaced with great care so that the replacement can attach itself to the bone that is still in the body. It is known that nanostructured hard tissue such as bone allows the surfaces of implants to attach themselves to bone a lot quicker than existing surface profiles. This is because living cells have an affinity to nanostructured features. In this paper, a machining technique is described that easily removes bone without destroying the natural features of the bone so that implants can attach themselves to the bone on the nanoscale.

One technique that shows much promise in machining bone is ultrahigh-speed milling; this technique has been shown to produce micro- and nano-scale structures in the same way as a conventional machine tool produces macro-scale features. A special requirement of machining at such small scales is the need to increase the rotational speed of the cutting tool. The cutting speed of the cutting tool is given by the following equation:

$$V = r\omega \quad \text{(Eq 1)}$$

where V is the cutting velocity (m/s), r is the cutting tool radius (m), and ω is the rotational speed in (radians/s). From this relationship, it can be seen that as the cutter diameter is reduced in size to create micro and nano-scale features the rotational speed must dramatically increase to compensate for the loss of cutting speed at the micro and nano-scale. At the present time, the fastest spindle commercially available rotates around 360,000 rpm under load conditions.

Research is currently being undertaken to improve the performance of these spindles where the initial aim is to reach 1,000,000 rpm (Ref 1). Strain rates induced at these high speeds cause chip formation mechanisms to be significantly different than those at low speeds. Additionally, it is now possible to experiment at the extreme limits of the fundamental principles of machining at ultrahigh speed and at the micro- and nano-scales using the conventional theories of machining. This study discusses the use of these theories at the microscale and at high strain rates and discusses the development of a model of initial chip formation during high strain rate deformation at the microscale.

2. Structure of Cancellous Bone

At the lower extremities of density, cancellous bone appears to be a complex set of open pores. As density increases the rods of hard tissue spread and flatten, become platelike, and finally fuse to form the dense outlying structure at the surface of the bone. Cancellous bone grows in response to an applied stress. Trabeculae develop along principal stress directions in the loaded bone. These ideas have been measured in vivo of the strains exerted in the cortex of the calcaneus of sheep. The exhibition of directional and anisotropic properties yields special attention from a machining viewpoint. Also, the nature of the microstructure may well exaggerate the wear of very small cutting tools. At the microscale, cancellous bone is a composite of a fibrous, organic matrix of proteins mainly collagen, filled with inorganic calcium compounds such as crystalline hydroxyapatite, $Ca_{10}(PO_4)_6(OH)_2$, and amorphous calcium phosphate, $CaPO_3$. These compounds provide bone with its stiff-

M.J. Jackson and **G.M. Robinson,** Department of Mechanical Engineering Technology and Center for Advanced Manufacturing, Purdue University, West Lafayette, IN 47907-2021; **H. Sein** and **W. Ahmed,** Surface Coatings Research Group, Manchester Metropolitan University, Department of Chemistry and Materials, John Dalton Building, Chester Street, Manchester, M1 5GD, UK; and **R. Woodwards,** Maxillofacial Surgery Unit, North Manchester General Hospital, Crumpsall, Manchester, M8 5RB, UK. Contact e-mail: jacksomj@purdue.edu.

ness. The compositions of compact and cancellous bone are almost the same, i.e., 35% organic matrix, 45% calcium compounds, and the remainder water.

3. Theory of Micromachining

Following the development of equations proposed by Shaw (Ref 2), these expressions are applied to a 6 flute end milling cutter with a shank diameter of 1.59 mm, a cutting diameter of 700 μm, and a rotational speed of 250,000 rpm, or 26,180 rad/s. The rake angle α was equal to 7° with a clearance angle θ equal to 10° and a shear plane angle φ equal to 24°. The material to be cut was cancellous bovine femur, and the horizontal force F_h was calculated assuming that the mass of the tool is concentrated at radius r:

$$F_h = mr\omega^2 \quad \text{(Eq 2)}$$

In this case, m is the tool mass (kg), and r is the tool radius (m). Coefficients of friction between different materials have been investigated by Bowden and Tabor (Ref 3). They also describe methods to determine the coefficient of friction. Using the method of the inclined plane, the coefficient of friction of cancellous bovine femur on tungsten carbide and steel is in the range $\mu = 0.5$ to 0.6 under lubricating conditions, i.e., sliding on a plane coated with a saline solution. Using the following equation:

$$\beta = \tan^{-1}\mu \quad \text{(Eq 3)}$$

The friction angle β can then be determined under these conditions. It was found to be 30.96°. This is in excellent agreement with Merchant and Zlatin's nomograph (Ref 2). The vertical force F_V can be found using the relationship:

$$F_v = \frac{\mu F_h - F_h \tan\alpha}{1 + \mu \tan\alpha} \quad \text{(Eq 4)}$$

This was found to be 5.25 N. Again, referring to the Merchant and Zlatin's nomograph for the coefficient of friction, the value of F_h is independently predicted to be 5.33 N (Ref 2). The force tangential to the tool plane F is found to be:

$$F = F_h \sin\alpha + F_v \cos\alpha \quad \text{(Eq 5)}$$

F was determined as 6.66 N. The force normal to the tool plane N is provided using the equation:

$$N = F_h \cos\alpha - F_v \sin\alpha \quad \text{(Eq 6)}$$

where N was found to be 11.1 N. The force perpendicular to the shear plane F_s can now be determined by:

$$F_s = F_h \cos\phi - F_v \sin\phi \quad \text{(Eq 7)}$$

and was estimated to be 8.76 N. The force normal to the shear plane N_s is given by the equation:

$$N_s = F_v \cos\phi + F_h \sin\phi \quad \text{(Eq 8)}$$

where N_s is 9.61 N. Now the frictional force F_f is:

$$F_f = F_v \cos\alpha + F_h \sin\alpha \quad \text{(Eq 9)}$$

F_f is approximately 6.66 N. It is possible to check this value with Merchant and Zlatin's nomograph for frictional force (Ref 2). However, the values for F_h and F_v are so small that the extreme limits of the nomograph are being tested so it is difficult to give an accurate value for F_f. It is certain this value is below 10 N, which is in close agreement with the calculated answer. The shear stress τ is found using the following quotient:

$$\tau = \frac{F_s}{A_s} \quad \text{(Eq 10)}$$

which has a value of 1.8 GN/m^2. The direct stress ρ is found by applying the relationship:

$$\sigma = \frac{N_s}{A_s} \quad \text{(Eq 11)}$$

and σ is found to be 1.95 GN/m^2. The chip thickness ratio r is given by:

$$r = \frac{t}{t_c} \quad \text{(Eq 12)}$$

In Eq 12, t is the undeformed chip thickness (or depth of cut) and t_c is the measured chip thickness. The machining of bone was conducted at such a small scale that it is difficult to measure t. Therefore r was calculated using the equation:

$$r = \frac{\tan\phi}{\cos\alpha + \sin\alpha \tan\phi} \quad \text{(Eq 13)}$$

Equation 13 yields a value for r equal to 0.425, and therefore, $t = 4.25$ μm. This is in excellent agreement with Merchant and Zlatin's nomograph for shear angles and the calculation can be made in confidence (Ref 2). Shear strain γ is found from:

$$\gamma = \frac{\cos\alpha}{\sin\phi \cos(\phi - \alpha)} \quad \text{(Eq 14)}$$

γ was calculated to be 2.55, and this can be independently verified from Merchant and Zlatin's nomograph for shear strain (Ref 2), which yields a value of 2.51.The cutting velocity V is found using:

$$V = T_{td}\omega \quad \text{(Eq 15)}$$

From Eq 15, the cutting velocity V is 9.1 m/s. The chip velocity is found from applying the following equation:

$$V_c = \frac{\sin\phi}{\cos(\phi - \alpha)} \quad \text{(Eq 16)}$$

where V_c is equal to 3.9 m/s. This value can also be found from Eq 17:

$$V_c = rV \quad \text{(Eq 17)}$$

The two results are in agreement. The shear velocity V_s is given by:

$$V_s = \frac{V\cos\alpha}{\cos(\phi - \alpha)} \quad \text{(Eq 18)}$$

where V_s is calculated to be 9.5 m/s. V_s can also be found from:

$$V_s = \gamma V \sin\phi \quad \text{(Eq 19)}$$

Again, the two results are in agreement. The strain rate $\dot{\gamma}$ is given by:

$$\dot{\gamma} = \frac{V\cos\alpha}{\Delta y \cos(\phi - \alpha)} \quad \text{(Eq 20)}$$

In Eq. 20, Δy is the shear plane spacing and $\dot{\gamma}$ is found to be 833 s^{-1}. The feed rate is 1 mm/min under experimental conditions and the feed per tooth δ is given by:

$$\delta = \frac{F_r}{N\omega} \quad \text{(Eq 21)}$$

N is equal to the number of teeth. Therefore, Δ is 6.66 μm and the scallop height is found by using the following equation:

$$h = \frac{\delta}{\left(\frac{4T_{td}}{\delta}\right) + \left(\frac{8N}{\pi}\right)} \quad \text{(Eq 22)}$$

Therefore, h is calculated to be 1.59×10^{-11} m under the experimental machining conditions.

4. Initial Chip Curl Modeling

Chip curvature is a highly significant parameter in machining operations from which a continuous chip is produced. In this study, observations are made on initial chip curl in the simplified case of orthogonal cutting at the micro- and nanoscales. The cutting process may be modeled using a simple primary shear plane and frictional sliding of the chip along the rake face. When the region of chip and tool interaction at the rake face is treated as a secondary shear zone and the shear zones are analyzed by means of slip-line field theory, it is predicted that the chip will curl. Thus, chip curvature may be interpreted as the consequence of secondary shear. Tight chip curl is usually associated with conditions of good rake face lubrication (Ref 4). At the beginning of the cut, a transient tight curl is often observed, with the chip radius increasing as the contact area on the rake face grows to an equilibrium value. Thus, it might be suggested that tight curl is an integral part of the primary deformation.

The process of continuous chip formation is not uniquely defined by the boundary conditions in the steady state and that the radius of curl may depend on the build-up of deformation at the beginning of the cut (Ref 4). A treatment of primary chip formation at the microscale is presented, which considers chip curl as a series of heterogeneous elements in continuous chip formation at the microscale. The free surface of the chip always displays lamellae, which are parallel to the cutting edge. The chip usually forms through a regular series of discrete shear events, giving a straight chip made up of small parallel segments. However, no account is taken of the bone material that moves past the tool between shear events. The following observations follow from Doyle, Horne, and Tabor's analysis of primary chip formation (Ref 4).

Figure 1 shows the instabilities during chip formation that gives rise to primary chip curl. The shaded range in Fig. 1(b) is the consequence of a built-up edge that very quickly becomes part of the segmented chips shown in Fig. 1(d). This material provides the means to curl the chip, and as a consequence of this event, the following model is presented. Previous treatments of chip curl analysis have focused on chip formation with a perfectly stiff cutting tool (Ref 5). However, during the machining of bone it is observed that the cutting tool bends as it cuts (Ref 6). This means that primary chip curl models must account for deflection of the cutting tool by bending during an orthogonal machining operation. Computational approaches to modeling chip formation at the micro and nanoscales have been attempted in recent years by a number of researchers (Ref 7, 8), who have used a molecular dynamics simulation approach using stiff cutting tools.

The generation of a transient built-up edge ahead of the cutting tool between shearing events in a bulging type of motion generates the shape of the segment of the metal chip. This is shown in Fig. 1(c), with the built-up edge forming the shaded triangle above the shear plane. If it is assumed that the built-up edge does not escape under the tool edge, then the areas of the shaded triangles in Fig. 1(b) and (c) will be equal. The chip moves away from the rake force in a manner shown in Fig. 1(d). The radius of chip curl can be calculated by assuming that the built-up edge is transient and that the element of the bulged material contains a small angle relative to the tool and workpiece. This angle will inevitably change during the bending action of the cutting tool. With reference to Fig. 2, if it is assumed that the cutting tool moves from point *A* to point *D*, the shear plane *AC* rotates to position *HC* as the built-up edge from triangle *ABD* is pushed into the segment of the chip. At point *D*, the shear along *DF* begins and segment

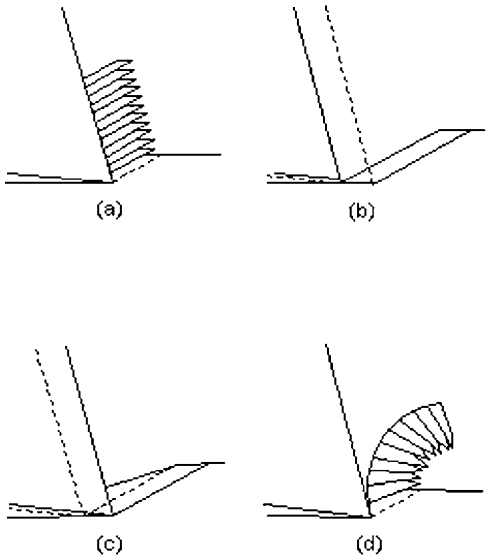

Fig. 1 Instability during the formation of a chip during micromachining: (a) segmented, continuous chip, (b) chip forming instability due to built-up edge, (c) movement of a built-up edge to form a chip, (d) serrated, continuous chip curl

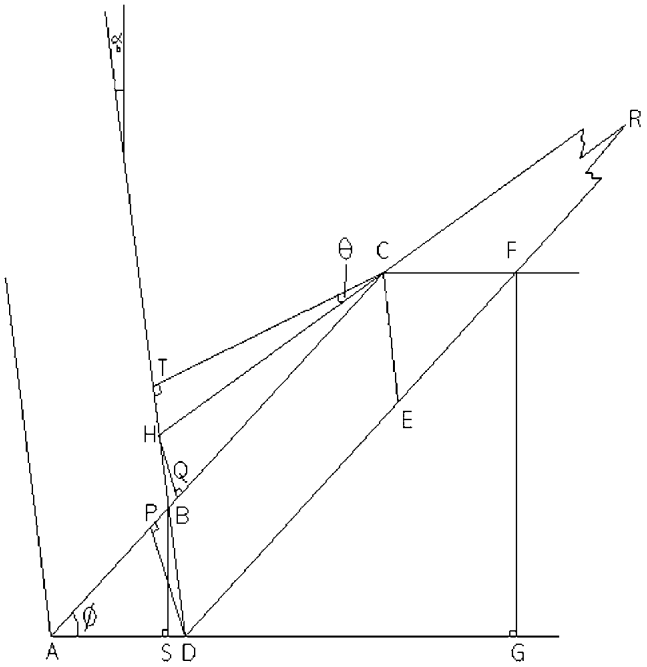

Fig. 2 Schematic diagram of the geometry of the primary chip that forms a curled chip

DHCF is completed. *HC* and *DF* meet at *R*, the center of the circle of the chip segment. Since the angle *HRD* is small, *RD* may be referred to as the radius of the chip. The clearance angle is θ.

Triangles *ABD* and *HBC* are equal in area and the depth of cut *FG* is equal to *d*. The spacing between the segments, i.e., the lamellae, is *CE*, which is equal to *BD*, which is equal to *s*. The chip thickness between lamellae, *TC*, is equal to *t*, while the rake angle SBD is equal to α. The cutting tool bends when machining at the microscale, which reduces the effective rake angle to α_b. Since the chip radius *r* can be taken as *RD*, while the shear angle subtended is $B\hat{A}D$, or *f*, the calculation of the chip radius is provided by the following analysis,

$$DP = s\cos(\phi - \alpha_b) \quad \text{(Eq 23)}$$

or

$$AB = \frac{BS}{\sin\phi} \quad \text{(Eq 24)}$$

$$BS = s\cos\alpha_b \quad \text{(Eq 25)}$$

Thus,

$$DF = AC = \frac{d}{\sin\phi} \quad \text{(Eq 26)}$$

and

$$AB = \frac{s\cos\alpha_b}{\sin\phi} \quad \text{(Eq 27)}$$

Now,

$$BC = AC - AB = \frac{d}{\sin\phi} - \frac{s\cos\alpha_b}{\sin\phi} \quad \text{(Eq 28)}$$

Therefore,

$$BC = \frac{(d - s\cos\alpha_b)}{\sin\phi} \quad \text{(Eq 29)}$$

The areas of Δ*ABD* and Δ*HBC* are equal, such that,

$$AB \cdot DP = HQ \cdot BC \quad \text{(Eq 30)}$$

Hence,

$$HQ = \frac{DP \cdot AB}{BC} = \frac{s\cos\alpha_b \cdot s\cos(\phi - \alpha_b)\sin\phi}{\sin\phi\,(d - s\cos\alpha_b)} \quad \text{(Eq 31)}$$

and thus,

$$HQ = \frac{s^2\cos\alpha_b \cdot \cos(\phi - \alpha_b)}{(d - s\cos\alpha_b)} \quad \text{(Eq 32)}$$

Also,

$$BH = \frac{HQ}{\cos(\phi - \alpha_b)} = \frac{s^2\cos\alpha_b}{(d - s\cos\alpha_b)} \quad \text{(Eq 33)}$$

and

$$DH = BH + BD = s + \frac{s^2\cos\alpha_b}{(d - s\cos\alpha_b)} \quad \text{(Eq 34)}$$

such that,

$$DH = \frac{sd}{(d - s\cos\alpha_b)} \quad \text{(Eq 35)}$$

Hence,

$$CH = \frac{TC}{\cos\theta} = \frac{t}{\cos\theta} \quad \text{(Eq 36)}$$

Therefore,

$$\sin H\hat{R}D = \sin H\hat{C}B = \frac{HQ}{HC} = \frac{s^2\cos\alpha_b \cdot \cos(\phi - \alpha_b) \cdot \cos\theta}{t\,(d - s\cos\alpha_b)} \quad \text{(Eq 37)}$$

and

$$\sin D\hat{H}R = \sin T\hat{H}C = \cos\theta \quad \text{(Eq 38)}$$

In triangle *HRD*,

$$\frac{RD}{\sin D\hat{H}R} = \frac{DH}{\sin H\hat{R}D} \quad \text{(Eq 39)}$$

Therefore,

$$RD = r = DH \cdot \frac{\sin D\hat{H}R}{\sin H\hat{R}D}$$
$$= \frac{sd}{(d - s\cos\alpha_b)} \cdot \frac{\cos\theta\, t\,(d - s\cos\alpha_b)}{s^2 \cos\alpha_b \cos(\phi - \alpha_b)\cos\theta} \quad \text{(Eq 40)}$$

Thus,

$$r = \frac{d\,t}{s\cos\alpha_b \cdot \cos(\phi - \alpha_b)} \quad \text{(Eq 41)}$$

If the width of the lamellae s is small compared with the chip thickness, then for continuous machining with a single shear plane,

$$\frac{d}{t} = \frac{\sin\phi}{\cos(\phi - \alpha_b)} \quad \text{(Eq 42)}$$

Hence,

$$\frac{t}{\cos(\phi - \alpha_b)} = \frac{d}{\sin\phi} \quad \text{(Eq 43)}$$

and so,

$$r = \frac{d^2}{s\cos\alpha_b \cdot \sin\phi} \quad \text{(Eq 44)}$$

Equation 44 predicts a positive chip radius at negative rake angles. The approximations considered in this model are appropriate when one considers that the model assumes that a secondary shear plane exists.

5. Experimental

5.1 Micromachining Apparatus

The machining of bovine femur was performed using a modified machining center. The bio-machining center was constructed to incorporate a high-speed air turbine spindle rated to operate at 360,000 rpm under no load conditions. When operating at relatively deep depths of cut, the speed of the spindle decreases to approximately 250,000 rpm. The table of the machine tool was configured to move in *x-y-z* coordinates by attaching a cross-slide powered by a direct current motor in all three principal axes. Each motor was controlled by a Motionmaster controller with a resolution as low as 500 nm. The cutting tools used were coated with diamond. The bio-machining center is shown in Fig. 3.

The bovine femur samples were machined at various depths of cut at high speed and were machined in an aqueous saline solution. The cutting tools were inspected at the end of all machining experiments using an environmental scanning electron microscope (ESEM). The measured spindle speed was 250,000 rpm during the machining experiments. The depth of cut ranged between 50 and 100 μm for all machining experiments. The machining feed rate was conducted at 5 mm/s (0.3 m/min). The microscale cutting tool was 700 μm in diameter and was associated with a cutting speed of 117 m/min at a machining feed rate of 0.3 m/min. The results of the experimental procedures are shown in Table 1.

The machined chips were examined in an ESEM where the lamellar spacing on each chip was determined. Transient chip curl was measured at the first 90° of tight chip curl. The curl radii was then compared with the calculated value derived using the idealized model, taking into account the degree of bending of the cutting tool.

5.2 Observations of Bone Chips

There are significant differences in the size and shape of chips when machined at medium and high speeds. This is especially so for biological materials such as cancellous bone. Figure 4 shows a collection of chips machined from bovine femur. It is seen in Fig. 4 that many of the particles are in fact chunks of material rather than nicely formed chips. It is possible that the chunks were formerly parts of larger chips that have since broken down and that chip thickness values should be recalculated based on the larger chip size. It can also be seen

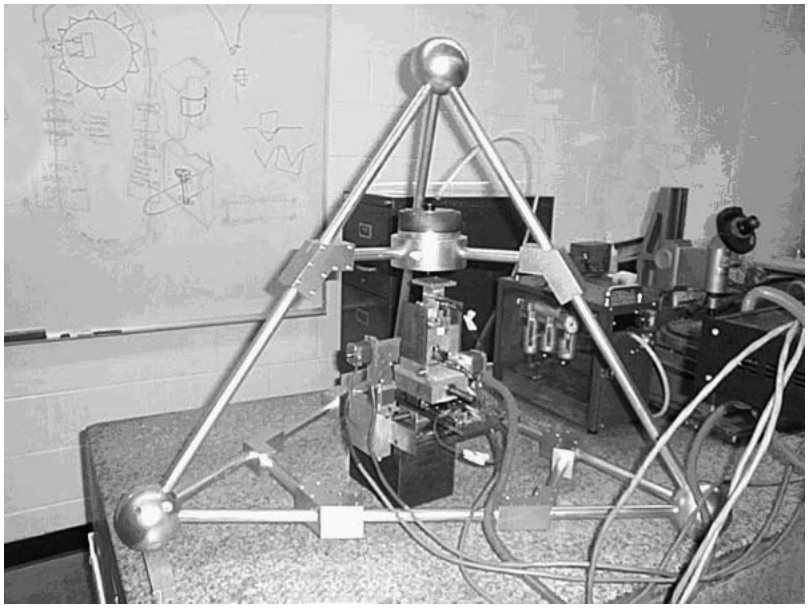

Fig. 3 Bio-machining center equipped with a high-speed air turbine spindle for rotating coated micro milling tools

that the chips in Fig. 4 are more consistent in terms of length, width, and depth. Their lamellar spacing is also regular in period, which would indicate that cutting conditions at high speed are stable. Single chip formations are shown in Fig. 5. While the width observed is similar to that for low speed cutting, the chip length of high-speed chips is much shorter than low speed chips. This could be because at low speed the chip has a greater time in contact with bone, thereby removing more material, which is reflected in the increased chip length.

One of the major differences between low and high speed bio-machining of bone is in the spacing of the lamellae. In low speed cutting, the chip spacing varies by a significant amount. However, at high cutting speeds the spacing is regular in period (Fig 6). At high speeds this process is accelerated to an extremely high level as the strain rate calculations have shown. In fact experiments show that chip types are similar in other materials such as metals. Figure 7 shows a magnified image of a coated cutting tool. The clearance faces of the flutes of the cutting tool show adherent bone chips with finely striated lamellae, as noted on the left hand side of the tool. Figure 8 shows a magnified image of a coated cutting tool detailing the cutting edge and its relationship to the adherent film of bovine femur showing fine striations of lamellae generated at high strain rates.

5.3 Bio-machining Results

The results of machining bovine femur at the microscale are compared with the model described for primary chip curl during the primary stages of chip formation. These results are presented in Table 1 for bone machined in an aqueous saline environment. Table 1 shows the results for bio-machining using a variety of rake angles. It should be noted that bending of the cutting tool produces a less acute rake angle when machining takes place. However, the shear plane angle is increased and larger chips are produced.

6. Discussion

It can be seen from the above analysis that despite the extremely high strain rates imposed due to high speed cutting, macro-scale equations can be applied accurately and produce impressive results. The most significant differences, however, appear in the following categories: strain rate, scallop height, and chip type. Many of the forces are similar in magnitude, offering no significant difference between macro-low speed and microhigh-speed machining. This is important during tool design as small tools must absorb the same impact forces as larger tools do during impact. However, when considering the strain rate, during microhigh speed machining the strain rate is 833 s^{-1} compared with the macro-low speed case of 667 s^{-1}. This is a 12.5 times increase, which relates directly to a 12.5 increase in speed from 20,000 to 250,000 rpm. Thus, the increase in strain rate is directly related to the increase in cutting speed. This is expected as the cutter imparts the strain and, therefore, a rate of strain to the material. The lamellae spacing Δy in Eq. 20 has a significant effect on the strain rate. Com-

Table 1 Experimental data comparing initial chip curl during bio-machining and initial chip curl predicted by the model; depth of cut, 100 μm

Rank angle after bending, °	Shear plane angle, °	Mean lamellar spacing, μm	Observed chip curl, mm	Calculated chip curl, mm
22	37	0.98	17.55	18.01
15	25	1.55	14.42	14.65
8	18	1.9	16.55	17.1
3	12	2.95	15.82	16.22

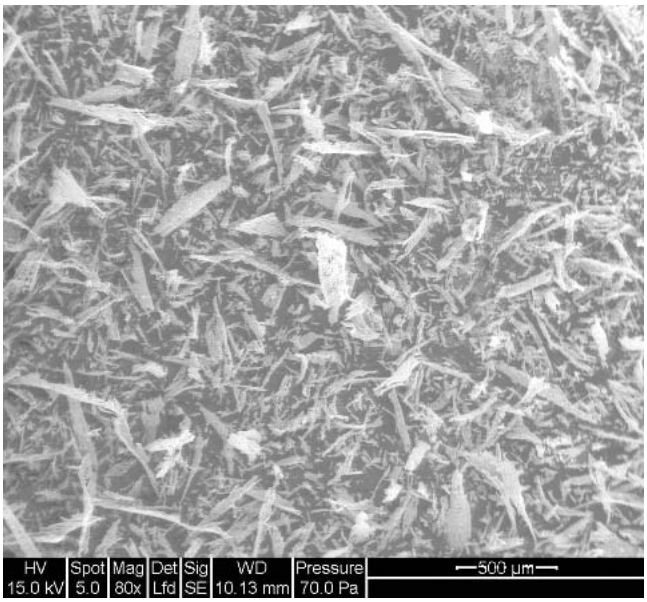

Fig. 4 Characteristic chip shapes cutting bovine femur at high speeds

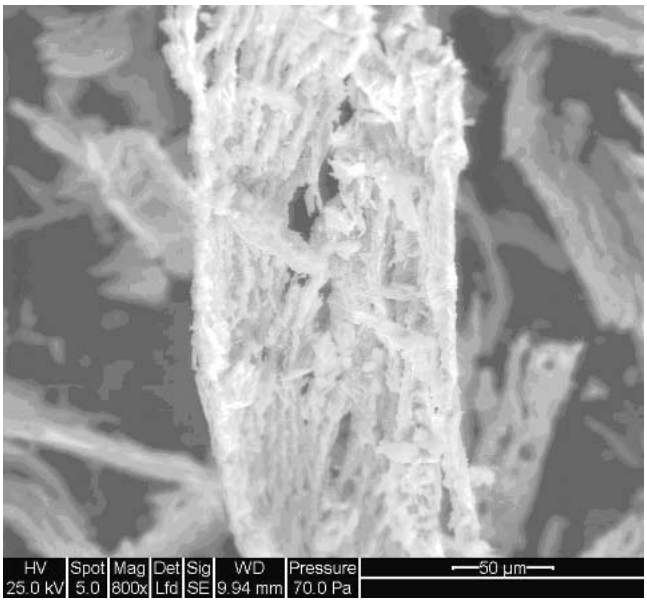

Fig. 5 Individual chip formation at high speed

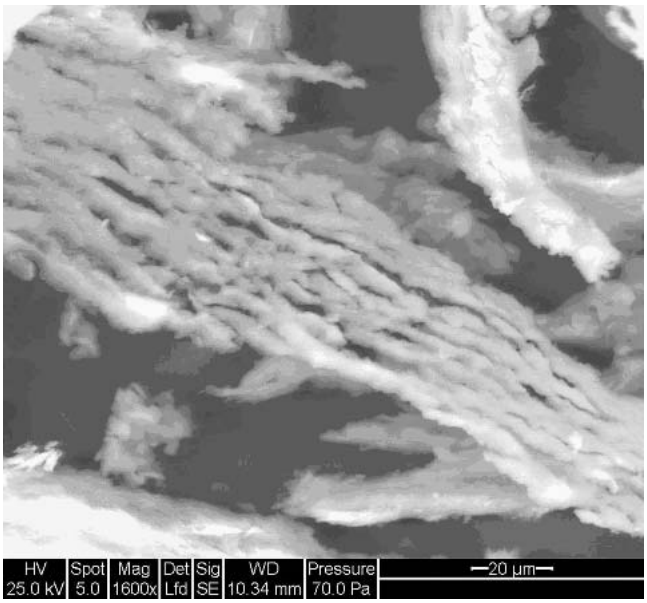

Fig. 6 Lamellae spacing of bovine femur at high speed

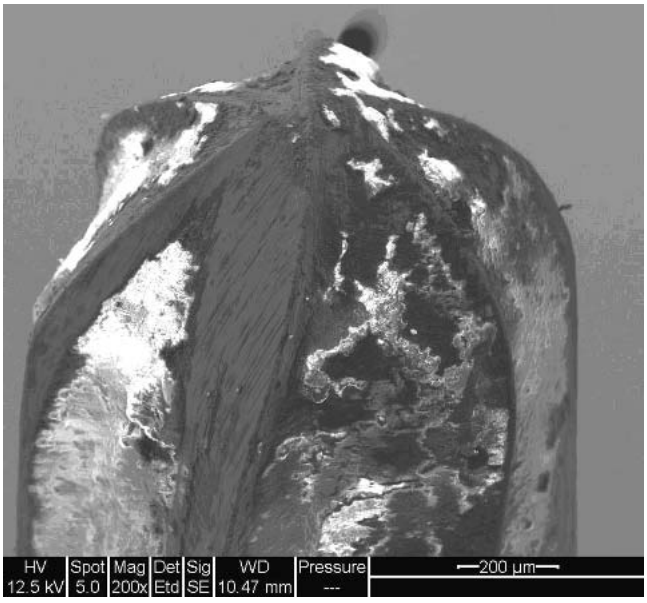

Fig. 7 Magnified image of the cutting tool showing cutting edges and adhered bone material

paring macro- and microscale chips, it is found that lamellae are ten times more closely packed in the high-speed chips than the low-speed chips.

The purpose of machining is to create useful surfaces, and hence, surface quality should be an important consideration of milling. Scallop height is a measure of this. An improvement is seen in the microhigh speed case with a scallop height of 1.58×10^{-11} m compared with 8.9×10^{-9} m for macro-slow speeds. Although both values seem insignificant, it must be remembered at the micro- and nano-scales, post-process finishing is inappropriate. Therefore, the surfaces created must meet specification without further processing. Additionally, due to the aspect ratio, small imperfections become serious defects at small scales. From the calculations, it can be seen that there is

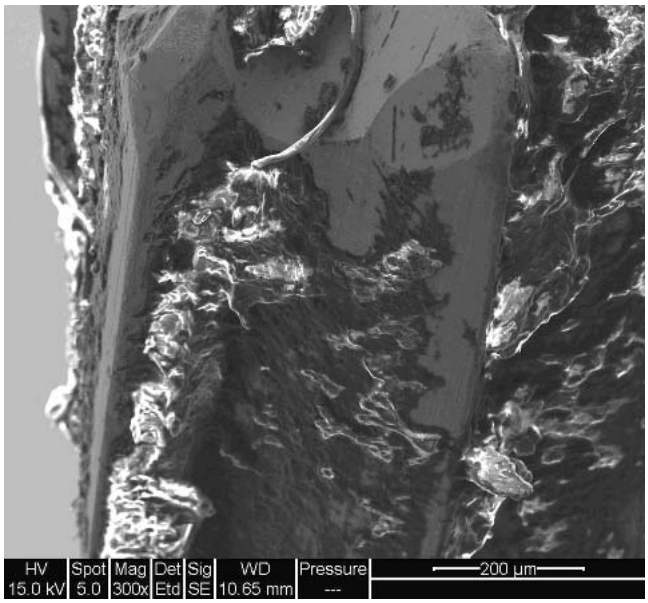

Fig. 8 View of cutting edges and adherent bovine femur chip showing fine striations of lamellae

an improvement in the scallop height, which is not the improvement required when considering the scale order of magnitude has changed by a factor of four. This is because the current spindle speeds reached are not high enough for effective machining, even if the speed is increased to 1,000,000 rpm. Thus, the orders of magnitude are increased further still.

The experimental results and observations provide an interesting view of machining bone at the microscale. When one considers the approximations made in the derivation of the chip curl model, the experimentally measured results compare well with the calculated chip curl. This indicates that cutting tool bending contributes significantly to initial chip curl prior to any significant frictional interactions on the rake face of the cutting tool. The proposed model describes the initial stages of chip curl quite well. If the description of chip curl is accurate, then continuous chip formation at the microscale needs to be reinvestigated. If one considers the movement of the cutting tool (Fig. 2), from point A towards point D, the shear plane is expected to oscillate between AC and HC depending on the amount of energy required to move the built-up edge into the segment of the subsequent chip. The cycle begins again when accumulated material is deposited on to the edge of the cutting tool and then onto the subsequent segment of the chip produced during machining.

7. Conclusions

The equations of metal cutting can be applied in the high-speed microscale environment. The nomographs of Merchant and Zlatin (Ref 2) can be applied, confirming that future calculations can be compared with these well-constructed charts. High strain rates change the mechanism of chip formation, thereby altering the shape of the chip. Also, high strain rates appear to provide less dependence on material properties in determining chip formation and shape.

A model of chip curl at the microscale has been developed and agrees well with experimental data. It appears that the

bending of the cutting tool contributes significantly to the primary chip prior to significant frictional interactions on the rake face of the cutting tool. It is shown that primary chip curl is initiated by the amount of material deposited onto the cutting tool, manifesting itself as a wedge angle that controls the amount of material pushed into the base of the segment of the chip between oscillations of the primary shear plane. Further studies on chip formation at the atomic scale are needed to develop nano-manufacturing processing methods for biological materials such as bone. The future development of this technique lies in the ability to rotate cutting tools at extremely high spindle speeds.

References

1. K. Kanjarkar, J. Cui, and M.J. Jackson, Design and Analysis of High-Speed Spindles for Nanomachining Applications Using a Computational Fluid Dynamics Approach, *Proceedings of the ASME South Eastern Region XI Technical Journal,* Vol 3 (No. 1), 2004, p 1.1-1.8
2. M.C. Shaw, *Metal Cutting Principles,* 2nd ed., Oxford Science Publications – Series on Advanced Manufacturing, Clarendon Press, University of Oxford, Oxford, UK, 2005, p 19
3. F. P. Bowden and D. Tabor, *The Friction & Lubrication Of Solids,* Oxford Science Publications, Clarendon Press, University of Oxford, Oxford, UK, 2001, p 73-75, 83-85
4. E.D. Doyle, J.G. Horne, and D. Tabor, Frictional Interactions between Chip and Rake Face in Continuous Chip Formation, *Proc. R. Soc. London,* Vol A366, 1979, p 173-183
5. I.S. Jawahir and J.P. Zhang, An Analysis of Chip Formation, Chip Curl and Development, and Chip Breaking in Orthogonal Machining, *Trans. North Amer. Manuf. Res. Inst. – Soc. Manuf. Eng.,* Vol 23, 1995, p 109-114
6. C.J. Kim, M. Bono, and J. Ni, Experimental Analysis of Chip Formation in Micro-milling, *Trans. North Amer. Manuf. Res. Inst.-Soc. Manuf. Eng.,* Vol 30, 2002, p 247-254
7. R. Komanduri, N. Chandrasekaran, and L.M. Raff, Molecular Dynamics Simulation of the Nanometric Cutting of Silicon, *Philos. Mag.,* Vol B81, 2001, p 1989-2019
8. X. Luo, K. Cheng, X. Guo, and R. Holt, An Investigation into the Mechanics of Nanometric Cutting and the Development of Its Test Bed, *Int. J. Prod. Res.,* Vol 41, 2003, p 1449-1465